Journal of Geophysical Research: Atmospheres

Supporting Information for

Laboratory Experiments on Savannah and European Boreal Forest Fire Emissions

V. Vakkari[1,2], L. Vettikkat[3], S. Kommula[3], A. Mukherjee[3], L. Hao[3], J. Backman[1], A. Buchholz[3], N. Gawlitta[4,†], M. Ihalainen[5], K. Jaars[2], K. Köster[6], V. Le[1], P. Miettinen[5], A. Nissinen[3], H. Czech[4,7], M. Alton[3,‡], J. Passig[7], S. Peltokorpi[3], A. A. Piedehierro[1], I. Pullinen[3], E. I. Rosewig[7], S. Schobesberger[3], D. Shukla[4,7], S. J. Siebert[8], M. Somero[5], A. Virkkula[1], A. Welti[1], P. Yli-Pirilä[5], A. Ylisirniö[3], R. Zimmermann[4,7], P. G. van Zyl[2], A. Virtanen[3] and O. Sippula[5,9]

[1]Finnish Meteorological Institute, Helsinki, Finland.
[2]Atmospheric Chemistry Research Group, Chemical Resource Beneficiation, North-West University, Potchefstroom, South Africa.
[3]Department of Technical Physics, University of Eastern Finland, Kuopio, Finland.
[4]Joint Mass Spectrometry Centre, Comprehensive Molecular Analytics, Helmholtz Zentrum München, Germany.
[5]Department of Environmental and Biological Sciences, University of Eastern Finland, Kuopio, Finland.
[6]Department of Environmental and Biological Sciences, University of Eastern Finland, Joensuu, Finland.
[7]Joint Mass Spectrometry Centre, Chair of Analytical Chemistry, University Rostock, Rostock, Germany.
[8]Unit for Environmental Sciences and Management, North-West University, Potchefstroom, South Africa.
[9]Department of Chemistry and Sustainable Technology, University of Eastern Finland, Joensuu, Finland.
†Current address: Analytical Chemistry Group, Department of Plant and Environmental Sciences, Faculty of Science, University of Copenhagen, 1871 Frederiksberg C, Denmark.
‡Current address: Aerodyne Research, Inc. Billerica, Massachusetts, USA.

Corresponding author: Ville Vakkari (ville.vakkari@fmi.fi)

Contents of this file

Introduction

Supporting text S1 describes emission factor (EF) calculation and error propagation for EFs for the BASFAA experiments. Supporting text S3 describes MAC_{OA} calculation. Supporting text S2 describes measurements, which were part of the BASFAA experiments but were not utilized in this study.

Text S1.

EF calculation and error propagation

For modified combustion efficiency (MCE) and EF calculation, ΔCO_2 is calculated from online sampling during the feeding ($CO_{2,online}$) as

$$\Delta CO_2 = \frac{CO_{2,online}\left(F_{dilution}+F_{sample}\right)-CO_{2,dilution}F_{dilution}}{F_{sample}} - CO_{2,room}, \quad \text{(S1)}$$

where $F_{dilution}$ is the dilution flow in the ejector diluter, F_{sample} is the sample flow in the ejector diluter, $CO_{2,dilution}$ is CO_2 concentration in the dilution air and $CO_{2,room}$ is CO_2 concentration in the room air. ΔCO and ΔCH_4 are calculated similar to Eq. (S1). For those experiments, when feed to the chamber consists of more than one continuous feeding, ΔCO_2 is calculated individually for every feed period and then an average weighted by sample volume is calculated.

Uncertainty in ΔCO_2 is estimated as

$$\sigma_{\Delta CO2} = \sqrt{\frac{(0.01\cdot CO_{2,online})^2\left(F_{dilution}+F_{sample}\right)^2+\sigma_{co2,picarro}{}^2F_{dilution}{}^2}{F_{sample}{}^2} + \sigma_{co2,room}{}^2}, \quad \text{(S2)}$$

where $\sigma_{CO2,picarro}$ is 20 ppb for cylinder air and twice that for compressed air, and $\sigma_{CO2,room}$ is the observed standard deviation of room air CO_2 approx. 10 minutes before ignition. Uncertainties for ΔCO and ΔCH_4 are calculated similar to Eq. (S2) and uncertainty in MCE is calculated as

$$\sigma_{MCE} = \sqrt{\frac{(\sigma_{\Delta CO2}\cdot\Delta CO)^2+(\sigma_{\Delta CO}\cdot\Delta CO_2)^2}{(\Delta CO_2+\Delta CO)^4}}. \quad \text{(S3)}$$

Measurements of CO concentration in the chamber before and after the sample feed are used to calculate $\Delta CO_{chamber}$ as

$$\Delta CO_{chamber} = (CO_{chamber,after} - CO_{chamb\ \ ,before})\cdot CO_{fraction}, \quad \text{(S4)}$$

where $CO_{fraction}$ is the fraction of combustion-originating CO in the feed into the chamber:

$$CO_{fraction} = \frac{\Delta CO}{CO_{online}}. \quad \text{(S5)}$$

Uncertainty in $CO_{fraction}$ is calculated as

$$\sigma_{COfraction} = \left|\frac{\Delta CO}{CO_{online}}\right|\sqrt{\frac{\sigma_{\Delta CO}{}^2}{\Delta CO^2} + \frac{(0.01\cdot CO_{online})^2}{CO_{online}{}^2}}. \quad \text{(S6)}$$

and uncertainty in $\Delta CO_{chamber}$ as

$$\sigma_{\Delta COchamber} = |\Delta CO_{chamber}|\sqrt{\frac{(2\sigma_{CO,picarro})^2}{(CO_{chamber,after} - CO_{chamber,before})^2} + \frac{(\sigma_{COfraction})^2}{CO_{fraction}{}^2}}. \quad \text{(S7)}$$

Emission ratios (ERs) of compounds measured from the chamber are calculated with respect to CO carbon concentration in the chamber (in μg m^{-3}) as

$$ER_X = \frac{X}{\frac{12.01 \cdot 101325}{8.31451 \cdot 273.15} \cdot \Delta CO_{chamber}}, \quad \text{(S8)}$$

where concentration X is also in units of μg m^{-3}. Uncertainty in ER_X is calculated as

$$\sigma_{ERX} = |ER_X|\sqrt{\frac{\sigma_X{}^2}{X^2} + \frac{\sigma_{\Delta COchamber}{}^2}{\Delta CO_{chamber}{}^2}}, \quad \text{(S9)}$$

where σ_X is the measurement uncertainty for concentration of compound X.

Text S2.

MAC_{OA} calculation and error propagation

Uncoated MAC_{BC} value of 7.5±1.2 m^2 g^{-1} at 550 nm wavelength (Bond and Bergstrom, 2006), is extrapolated to other wavelengths with AAE of 1.0 (Bond et al., 2013; Zotter et al., 2017). However, AAE of BC depends on microphysical properties such as core size, internal structure and coating (Gyawali et al., 2009; Virkkula, 2021; Luo et al., 2023) and therefore we include an uncertainty of ± 0.2 in the BC AAE for MAC_{BC}. Thus,

$$MAC_{BC}(\lambda) = \frac{550}{\lambda} \cdot 7.5 m^2 g^{-1}. \quad \text{(S10)}$$

Uncertainty in MAC_{BC} is estimated through Gaussian propagation as

$$\sigma_{MACBC} = |MAC_{BC}|\sqrt{\frac{1.2^2}{7.5^2} + \left|log(\frac{550}{\lambda})^{0.2}\right|^2}. \quad \text{(S11)}$$

Mass absorption coefficient of OA (MAC_{OA}) is estimated as

$$MAC_{OA}(\lambda) = \frac{\Delta b_{abs}(\lambda) - b_{abs,BC}(\lambda)}{\Delta OA}, \quad \text{(S12)}$$

where b_{abs} is the observed absorption coefficient at wavelength λ, and Δ indicates that chamber background before sample addition has been subtracted. $b_{abs,BC}$ is BC absorption coefficient calculated as

$$b_{abs,BC}(\lambda) = \Delta rBC \cdot MAC_{BC}(\lambda), \quad \text{(S13)}$$

and MAC_{BC} is calculated from Eq (S10). Uncertainty in $b_{abs,BC}$ is estimated through Gaussian propagation as

$$\sigma_{abs,bc} = \left|b_{abs,BC}\right| \sqrt{0.10^2 + \left(\frac{\sigma_{MACBC}}{MAC_{BC}}\right)^2} \quad \text{(S14)}$$

using 10 % uncertainty for rBC. Uncertainty in MAC_{OA} is then estimated through Gaussian propagation with measurement uncertainties of 35 % for b_{abs} and 20 % for OA as

$$\sigma_{MACOA} = \sqrt{\left(\frac{b_{abs}}{OA}\right)^2 (0.35^2 + 0.20^2) + \left(\frac{b_{abs,BC}}{OA}\right)^2 \left(\left(\frac{\sigma_{abs,bc}}{b_{abs,BC}}\right)^2 + 0.20^2\right)} . \quad \text{(S15)}$$

Text S3.

Additional measurements during the campaign

3.1 Off-line sampling

Off-line samples for gas phase organics of different volatilities were collected using adsorber tubes filled with three layers of graphitized carbon black (GCB) sorbents. Reactive sampling of carbonyl compounds (CCs) was done on cartridges packed with a DNPH (2,4-dinitrophenylhydrazine) sorbent supported on silica gel. Gillian GilAir Plus sampling pumps (Gilian, USA) were used for collecting samples at a controlled flow rate. After each primary and ageing experiment, the sampling tubes and cartridges were immediately removed from the sampling line, sealed with caps, and stored at -20°C until analysis. Targeted analyses using gas chromatography mass spectrometry (GCMS-QP2010 Ultra Shimadzu, Japan) equipped with thermal desorber unit (TDU-20, Shimadzu) for VOCs/IVOCs and high-performance liquid chromatography (HPLC, Agilent 1260 Infinity II, USA) with diode array detection (DAD) for CCs will be performed in other studies.

Primary and aged aerosol were collected on quartz fibre filters for off-line OC-EC analysis following IMPROVE-A protocol in an OC-EC analyzer (Lab OC-EC Aerosol Analyzer; Sunset Laboratory Inc.). Filter samples of primary and aged aerosol were extracted with water and methanol to obtain water-soluble organic compounds (WSOC) and methanol-soluble organic compounds (MSOC), respectively. Subsequently, the light absorption properties of WSOC and MSOC were estimated by recording their UV-vis spectra in the wavelength range of 250-700 nm using a spectrophotometer (UV-2401 PC, Shimadzu).

3.2 Cloud activating and ice nucleating properties

Cloud condensation nuclei (CCN) activity measurements were carried out with a CCN counter (CCNc, DMT model CCN-100). CCNc was operated in a setup for size-resolved

measurements, i.e. after a Vienna-type DMA and in parallel with a condensation particle counter (CPC, TSI model 3775). The DMA was operated with 0.8 LPM aerosol flow and 6.5 LPM sheath flow. The CCNc measurements covered a size range from 20 nm to 300-600 nm, where the upper limit of the size scan was chosen based on the number size distribution in the chamber. During primary measurements, CCNc size scans were performed at supersaturations of 0.43 %, 0.65 %, 0.87 %, and 1.1 %. During aging, additional supersaturations of 0.09 %, 0.2 %, and 0.31 % were used and 1.1 % was omitted. Duration of one size scan was 6-10 min and total duration of scans at all supersaturations was 36-52 min for primary and 54-78 min for aging measurements.

The ice nucleation efficiency of the biomass burning aerosol at cirrus cloud conditions were measured online using a modified SPectrometer for Ice Nuclei (SPIN) (Welti et al., 2020). SPIN measurements were performed on both size-selected particles and the entire polydisperse particle population emitted from the burns. Fresh and aged aerosol were measured. For selected experiments, the aerosol was subjected to a humidification-drying cycle before testing the ice nucleation efficiency to see if "warm cloud processing" had an impact. Particle filter and ash samples were also collected for offline analyses investigating conditions relevant for mixed-phase cloud formation. Overall, the generated biomass burning aerosol was not efficient at ice formation under either cirrus or mixed-phase cloud conditions.

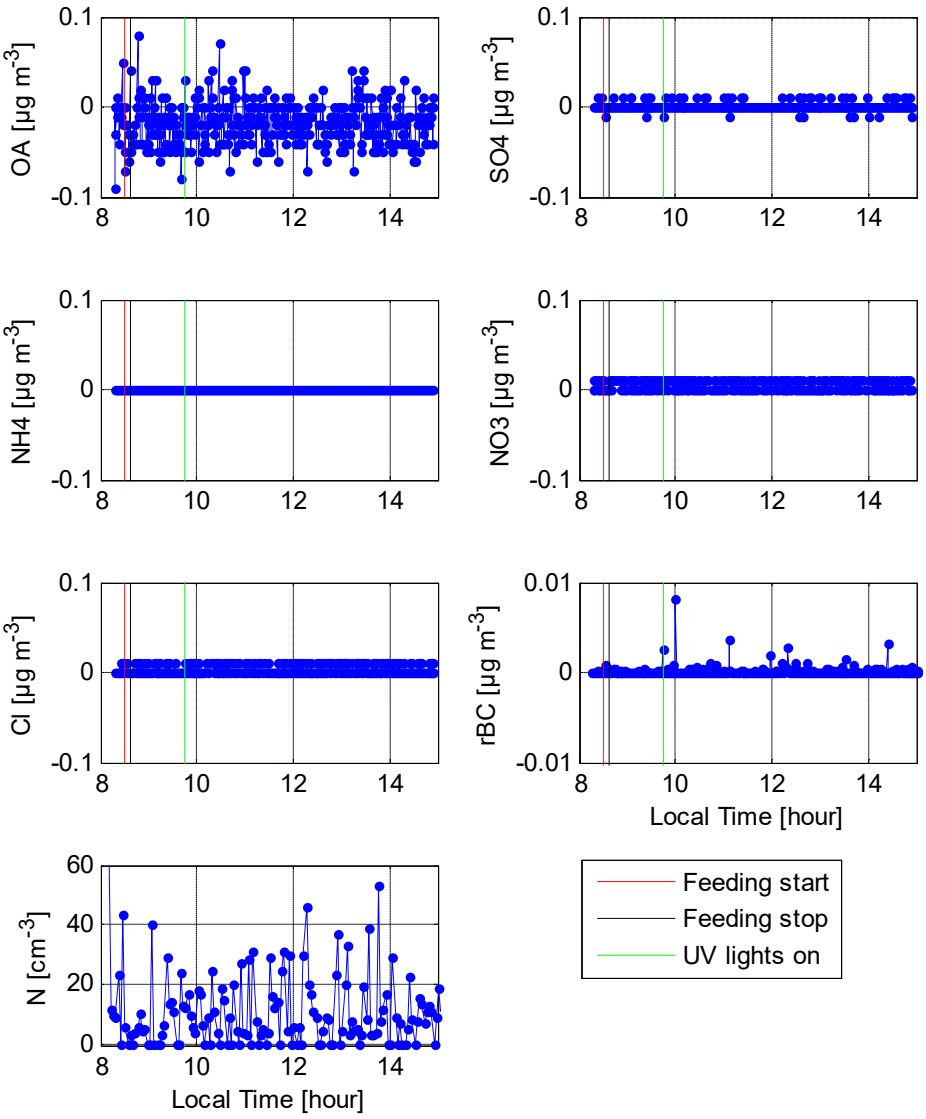

Figure S1. Time series of OA, SO4, NH4, NO3, Cl, rBC and total particle number concentration from SMPS during the blank experiment on 11 May 2022.

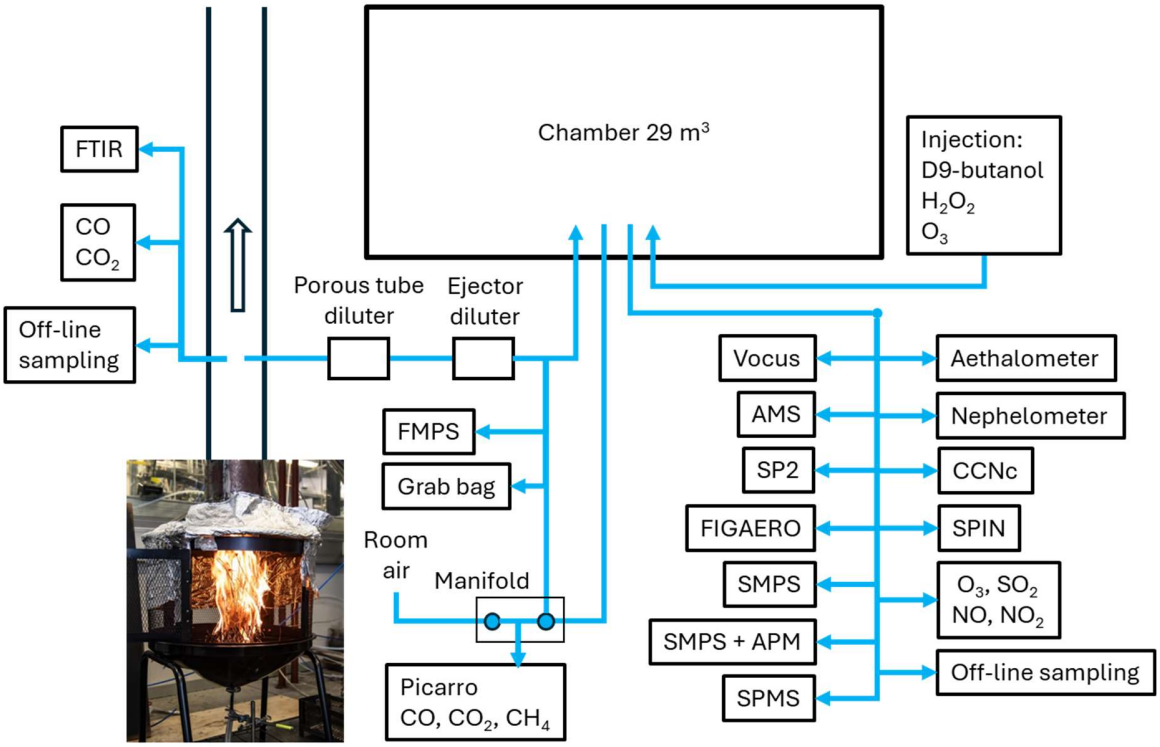

Figure S2. Schematic drawing of the measurement setup in BASFAA campaign. An example of savannah grass flaming combustion is pictured. Drawing is adapted from Mukherjee et al. (2025).

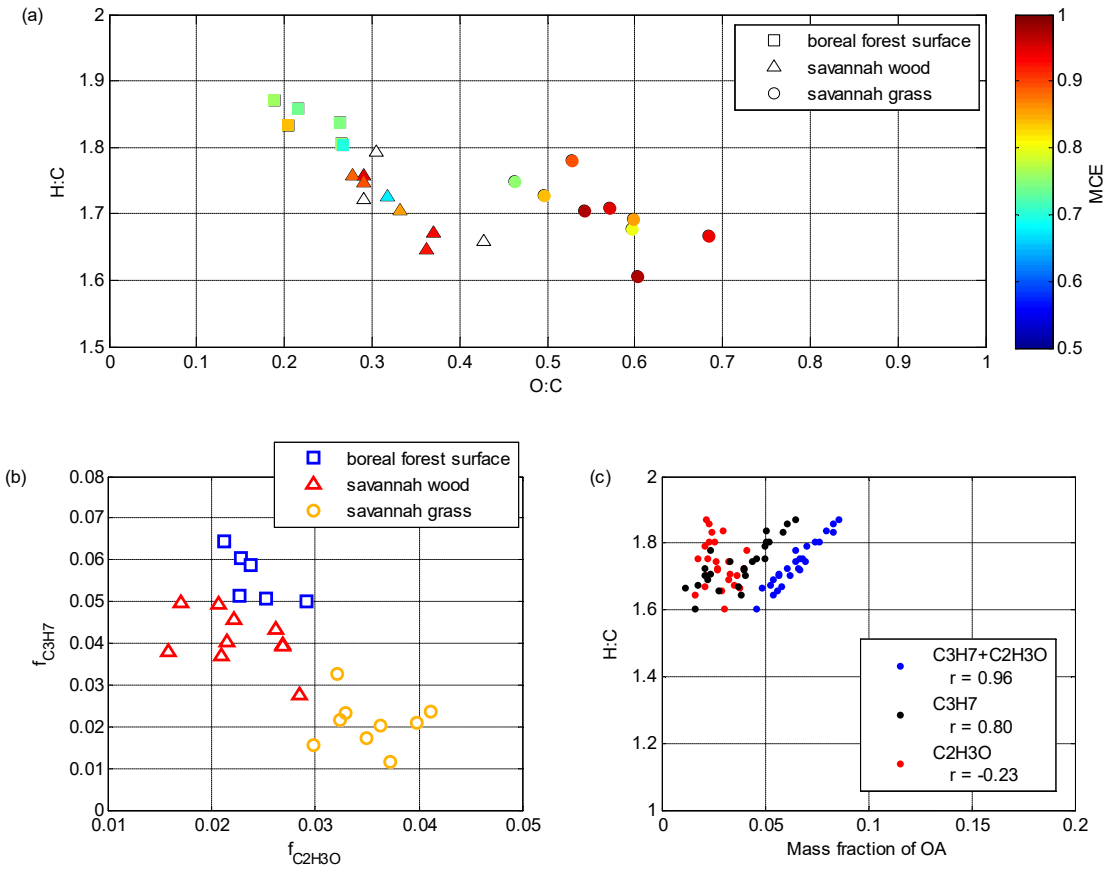

Figure S3. (a) H:C and O:C ratio for primary OA from AMS measurements. Colour indicates MCE. (b) OA mass fraction of ions $C_2H_3O^+$ and $C_3H_7^+$ for the different biomass types. (c) Pearson correlation of H:C ratio and mass fraction of different ions at m/z 43. The sum of $C_2H_3O^+$ and $C_3H_7^+$ covers on average 97 % of OA mass at m/z 43.

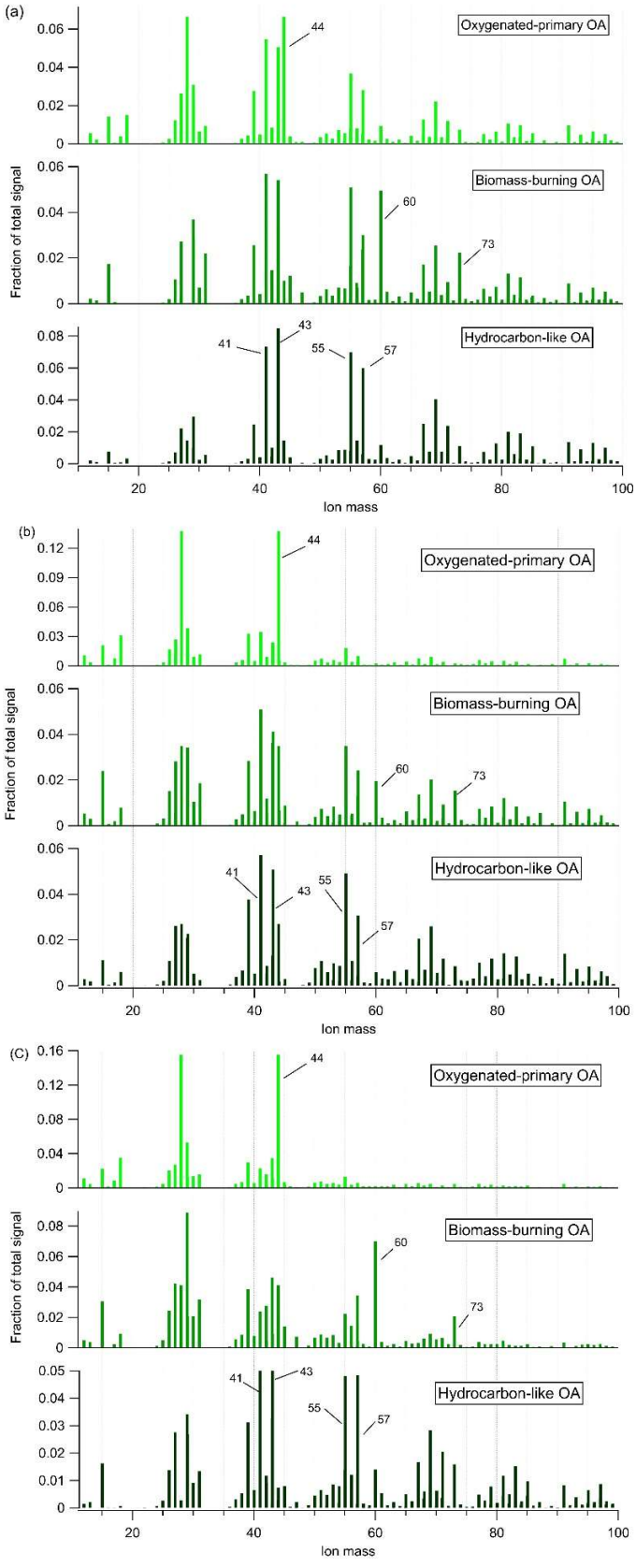
(a)
Oxygenated-primary OA
Biomass-burning OA
Hydrocarbon-like OA
Fraction of total signal
Ion mass
(b)
Oxygenated-primary OA
Biomass-burning OA
Hydrocarbon-like OA
Fraction of total signal
Ion mass
(C)
Oxygenated-primary OA
Biomass-burning OA
Hydrocarbon-like OA
Fraction of total signal
Ion mass

Figure S4. PMF mass spectra of the combined factor profiles for (a) boreal forest surface, (b) savannah wood, and (c) savannah grass.

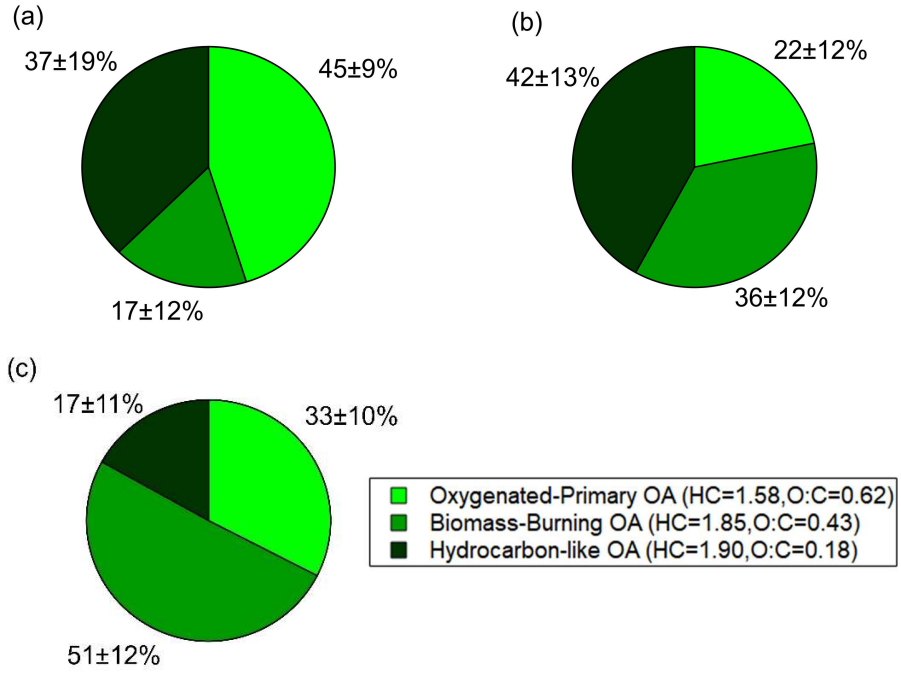

Figure S5. Average OA composition from PMF analysis of HR-organic mass spectra for primary emissions in (a) boreal forest surface, (b) savannah wood, and (c) savannah grass experiments.

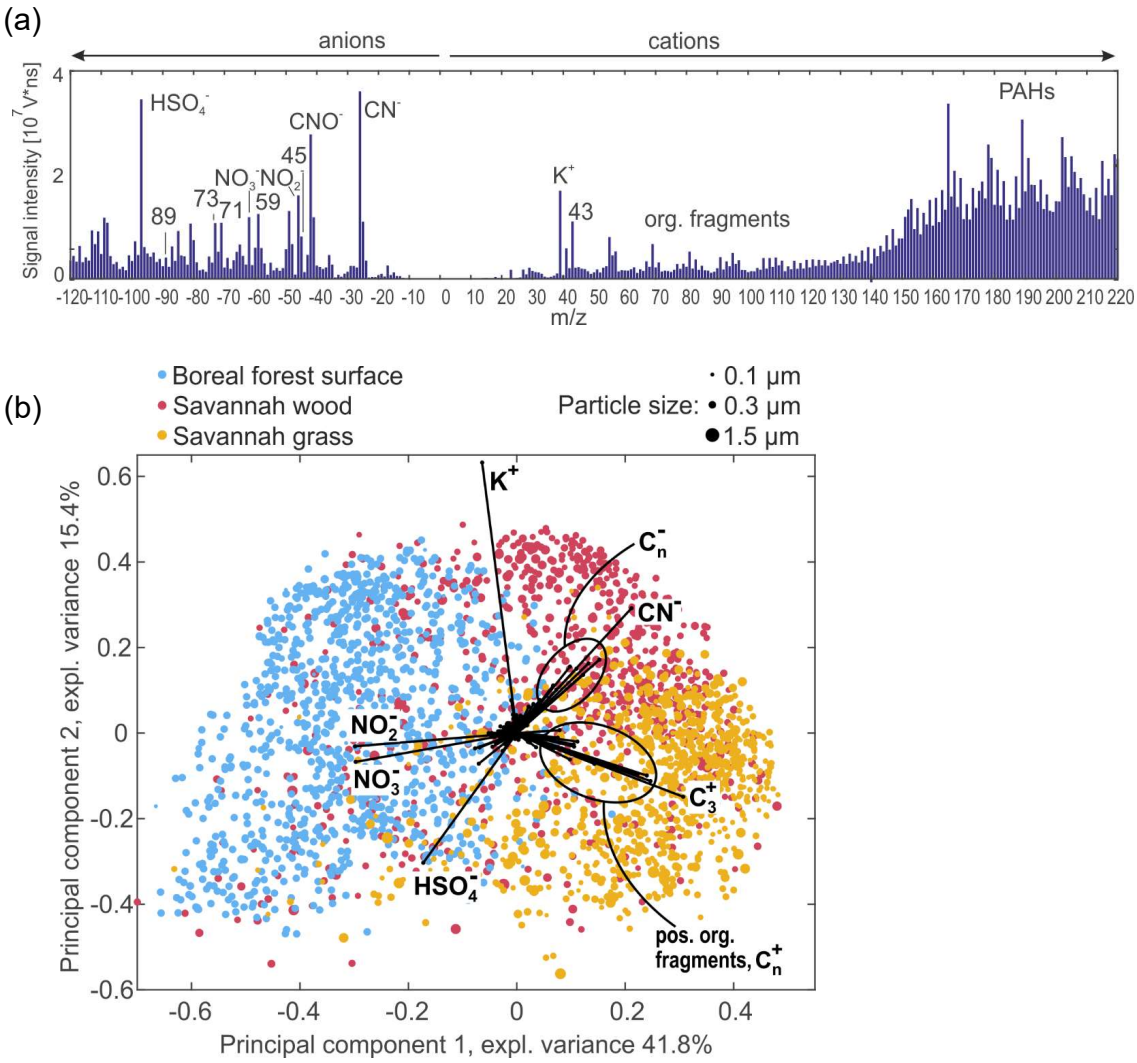

Figure S6. (a) Exemplary mass spectrum of fresh boreal forest floor emissions, averaged over 2,500 single-particle spectra. The SPMS system records both positive and negative ion spectra, capturing refractory materials, inorganics, and polycyclic aromatic hydrocarbons (PAHs). Numbers indicate oxygen-containing organic species and fragments. (b) Principal component analysis of single-particle mass spectra from laser desorption/ionization for Boreal forest surface (blue, MCE=0.84), Savannah wood (red, MCE=0.88) and Savannah grass (orange, MCE=0.84), each n=1,000 particles. Eigenvector lengths represent the contribution of signals at different m/z ratios to the variations in the mass spectrum. The mass spectra of particles from all fuels are dominated by organic fragments of rather similar composition (short eigenvectors at the center, not annotated) and therefore contribute little to the total signal variance. However, the inorganic composition varies across the fuels, e.g. with stronger K+ signals for savannah wood and increased sulphate signatures for boreal forest surface material.

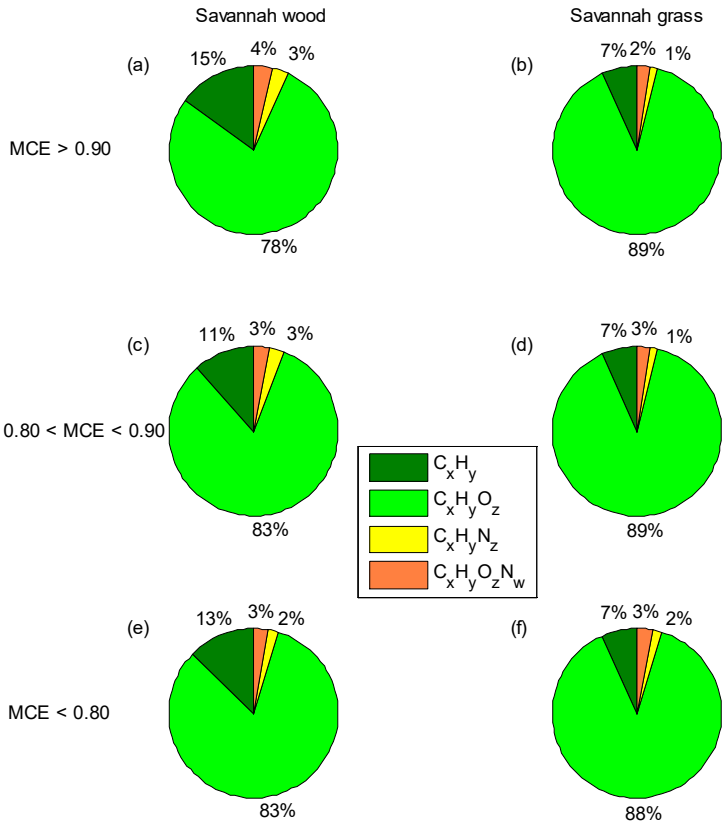

Figure S7. The average distribution of VOCs from Vocus measurements into hydrocarbons, oxygenated compounds and nitrogen containing compounds for savannah wood and grass experiments at certain MCE ranges. (a) Flaming combustion savannah wood experiments with MCE > 0.90. (b) Flaming combustion savannah grass experiments with MCE > 0.90. (c) Smouldering combustion savannah wood experiments with MCE ranging from 0.80 to 0.90. (d) Smouldering combustion savannah grass experiments with MCE ranging from 0.80 to 0.90. (e) Smouldering combustion savannah wood experiments with MCE < 0.80. (f) Glowing combustion savannah grass experiments with MCE < 0.8.

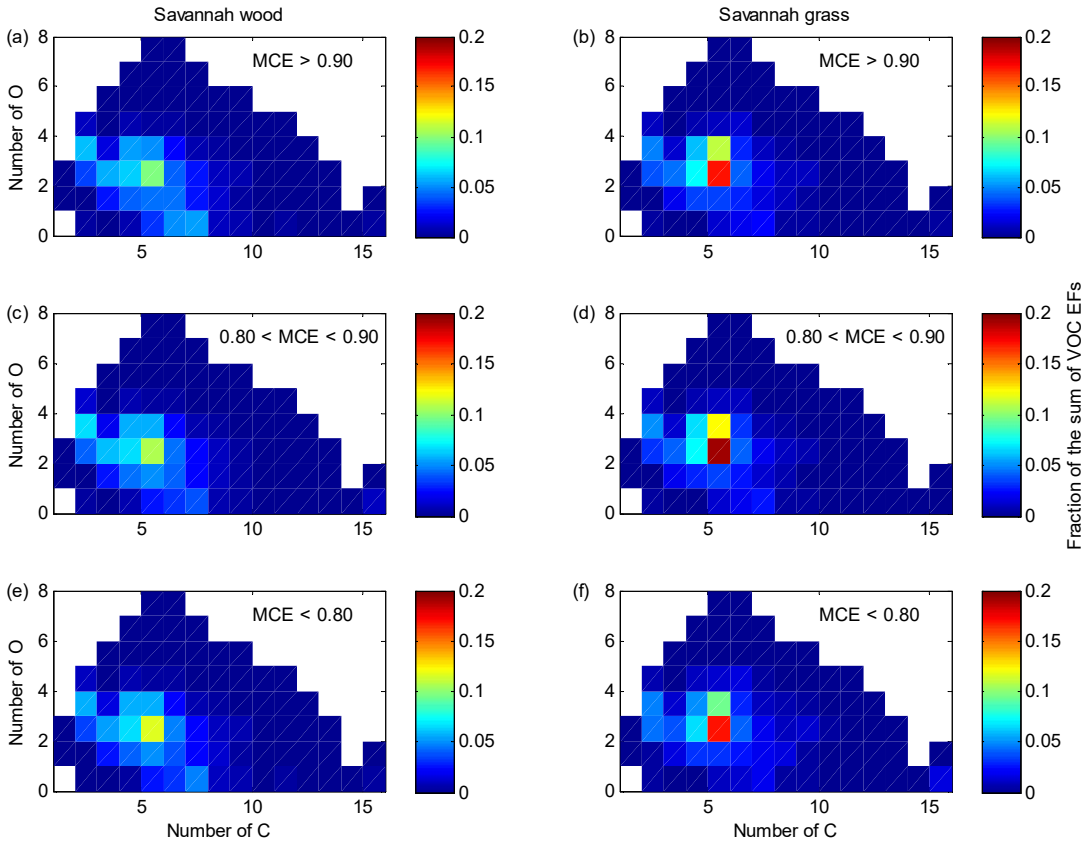

Figure S8. The fraction of total VOC EFs at a given number of O and C atoms for savannah wood and grass experiments at certain MCE ranges. (a) Flaming combustion savannah wood experiments with MCE > 0.90. (b) Flaming combustion savannah grass experiments with MCE > 0.90. (c) Smouldering combustion savannah wood experiments with MCE ranging from 0.80 to 0.90. (d) Smouldering combustion savannah grass experiments with MCE ranging from 0.80 to 0.90. (e) Smouldering combustion savannah wood experiments with MCE < 0.80. (f) Glowing combustion savannah grass experiments with MCE < 0.8.

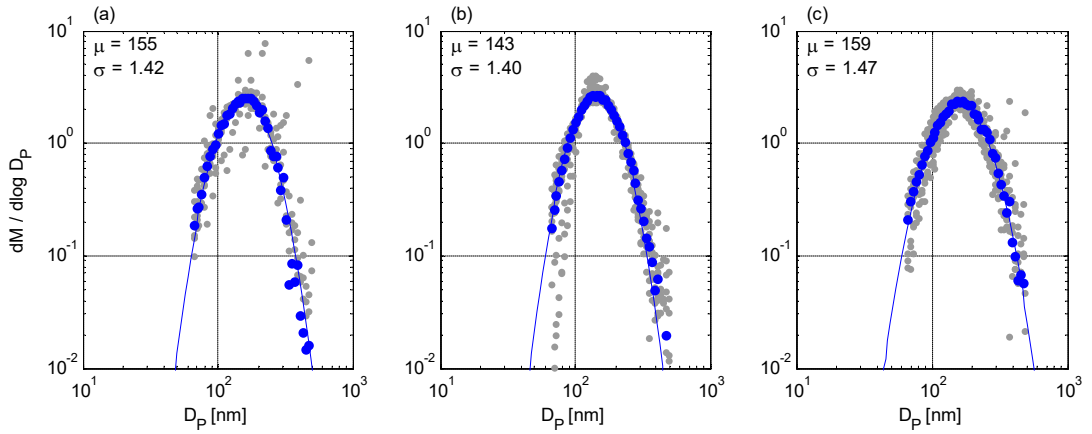

Figure S9. Median rBC mass distributions from SP2 measurements with unimodal log-normal fits. (a) Boreal forest surface. (b) Savannah wood. (c) Savannah grass. Individual experiments are indicated in grey.

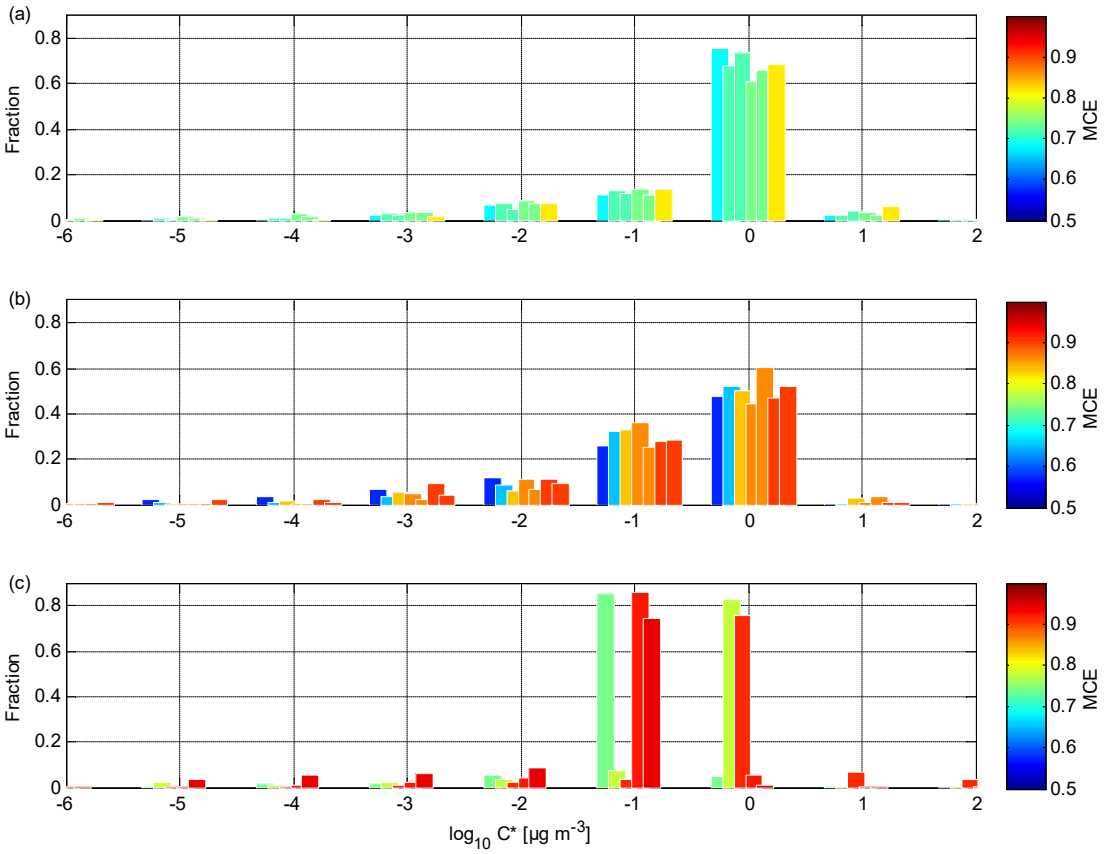

Figure S10. Particle phase volatility distributions from FIGAERO measurements, grouped logarithmically according to effective saturation vapor concentration (C*) as in Fig. 10, coloured with MCE. (a) Boreal forest surface. (b) Savannah wood. (c) Savannah grass.

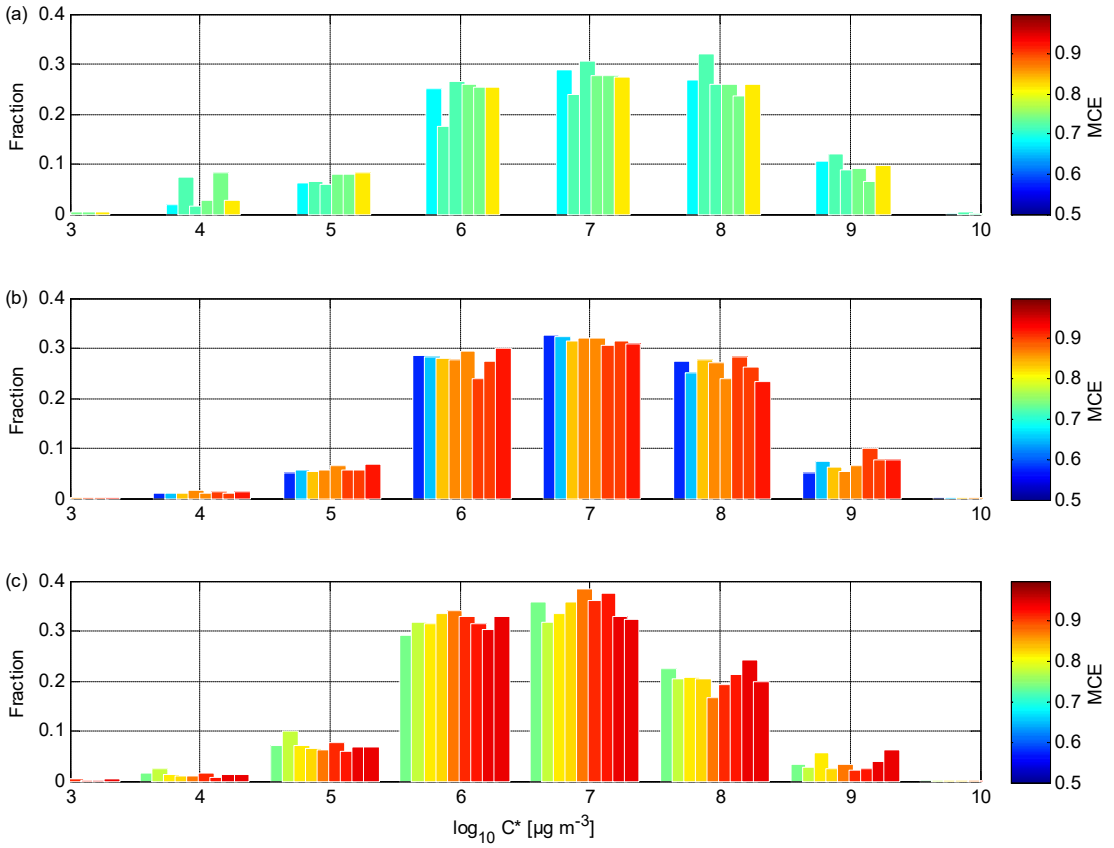

Figure S11. Gas phase volatility distributions from Vocus measurements, grouped logarithmically according to effective saturation vapor concentration (C*) as in Fig. 10, coloured with MCE. (a) Boreal forest surface. (b) Savannah wood. (c) Savannah grass.

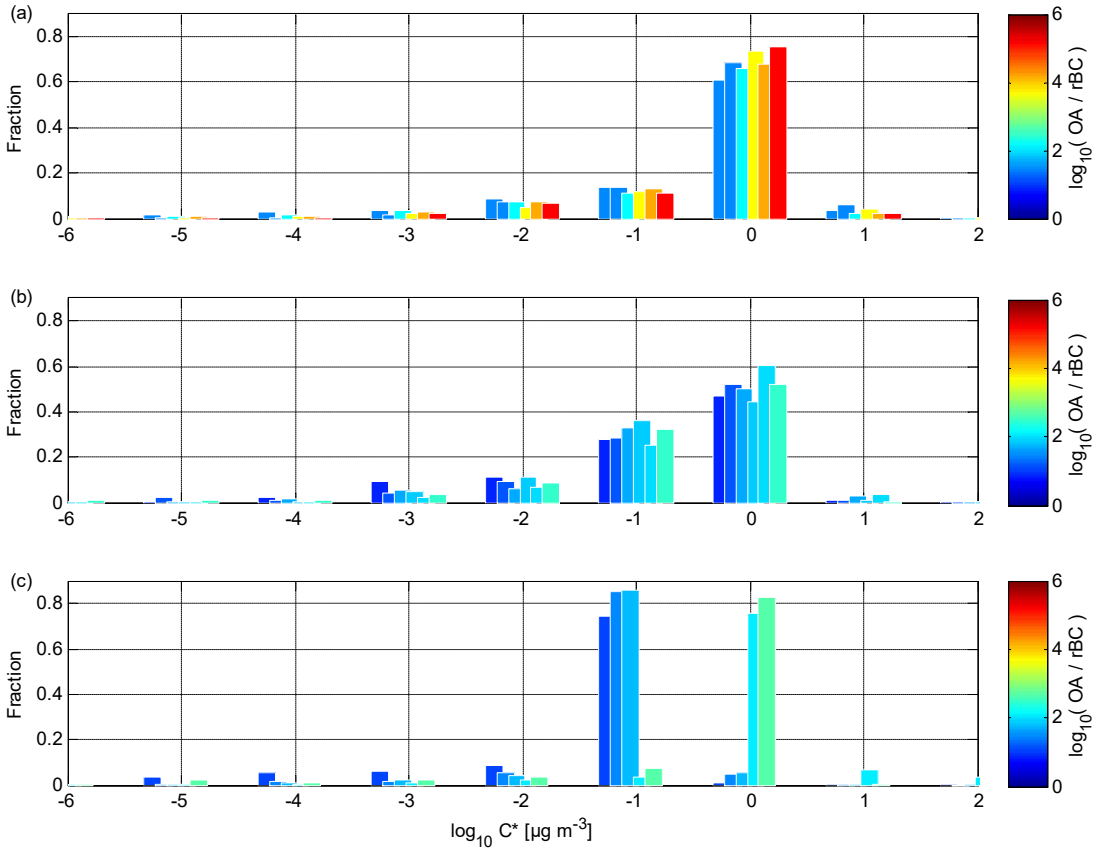

Figure S12. Particle phase volatility distributions from FIGAERO measurements, grouped logarithmically according to effective saturation vapor concentration (C*) as in Fig. 10, coloured with logarithm of OA/rBC ratio. (a) Boreal forest surface. (b) Savannah wood. (c) Savannah grass.

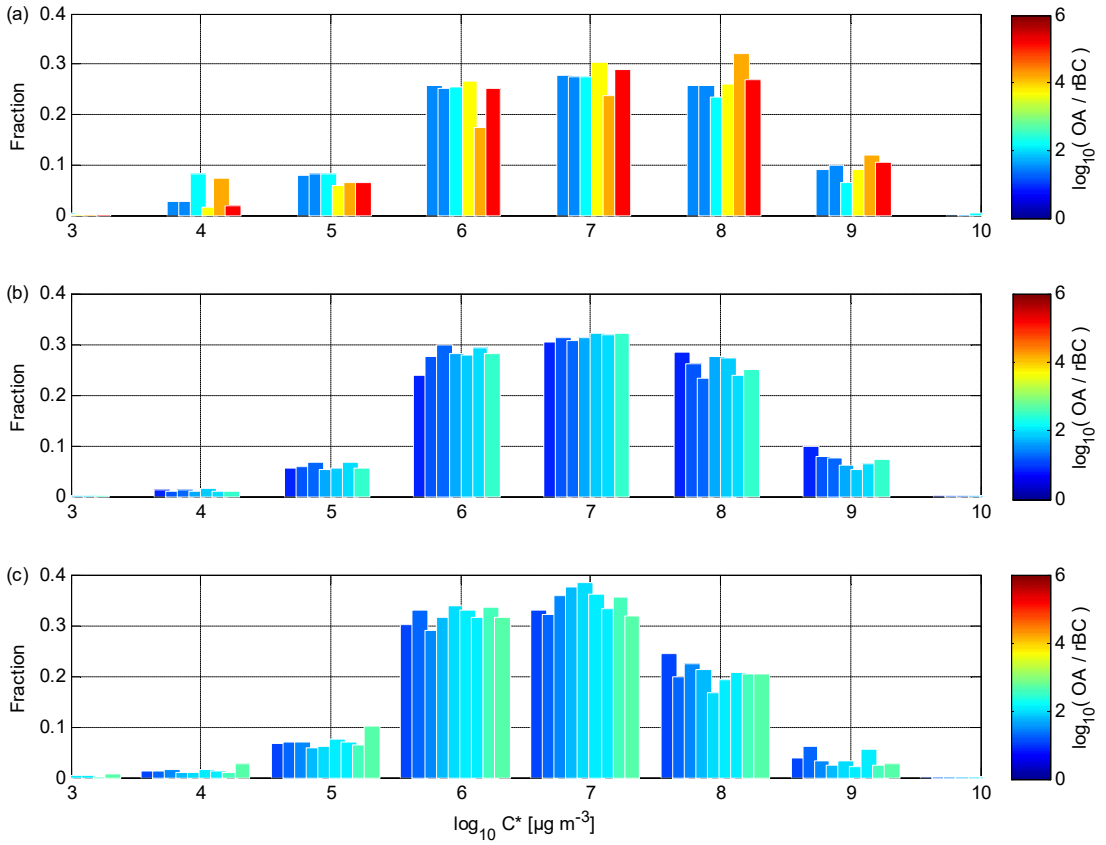

Figure S13. Gas phase volatility distributions from Vocus measurements, grouped logarithmically according to effective saturation vapor concentration (C*) as in Fig. 10, coloured with logarithm of OA/rBC ratio. (a) Boreal forest surface. (b) Savannah wood. (c) Savannah grass.

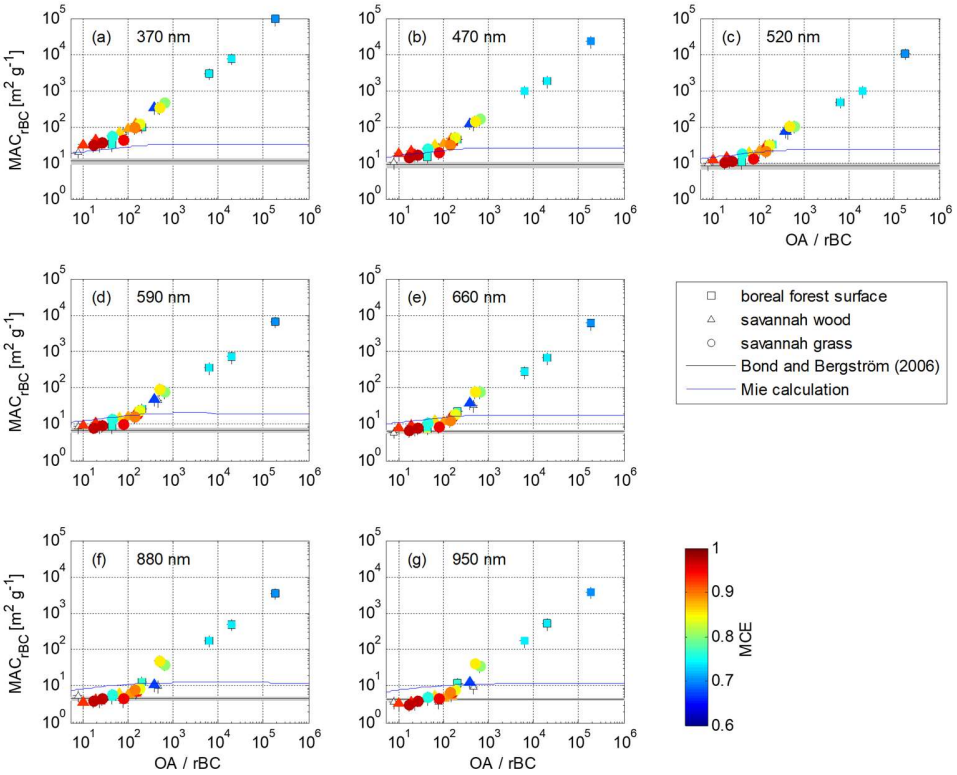

Figure S14. Observed MAC_{rBC} as function of OA/rBC ratio at different wavelengths. Error bars indicate measurement uncertainty. MAC_{BC} from Bond and Bergström (2006) is included with shaded area indicating uncertainty. The maximum absorption enhancement from coating on rBC core was estimated with Mie model calculations following Virkkula (2021).

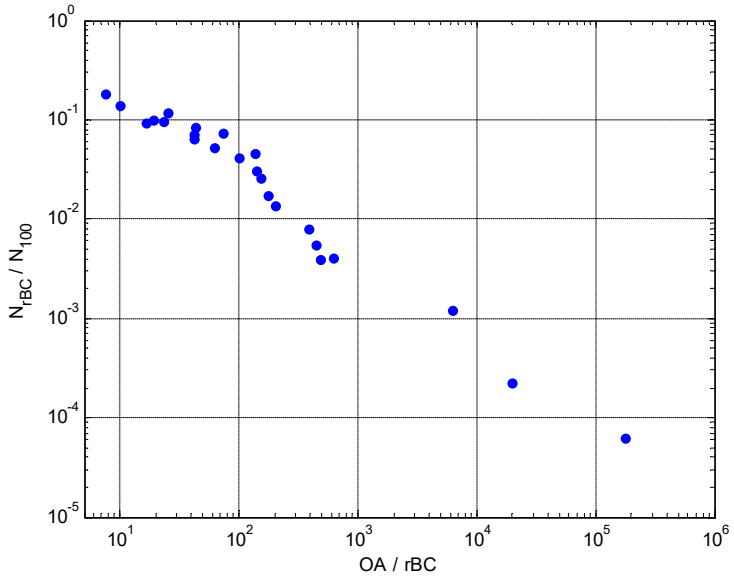

Figure S15. Ratio of number concentration of rBC-containing particles measured by SP2 to number concentration of particles larger than 100 nm in diameter from SMPS measurements as a function of OA to rBC mass concentration ratio.

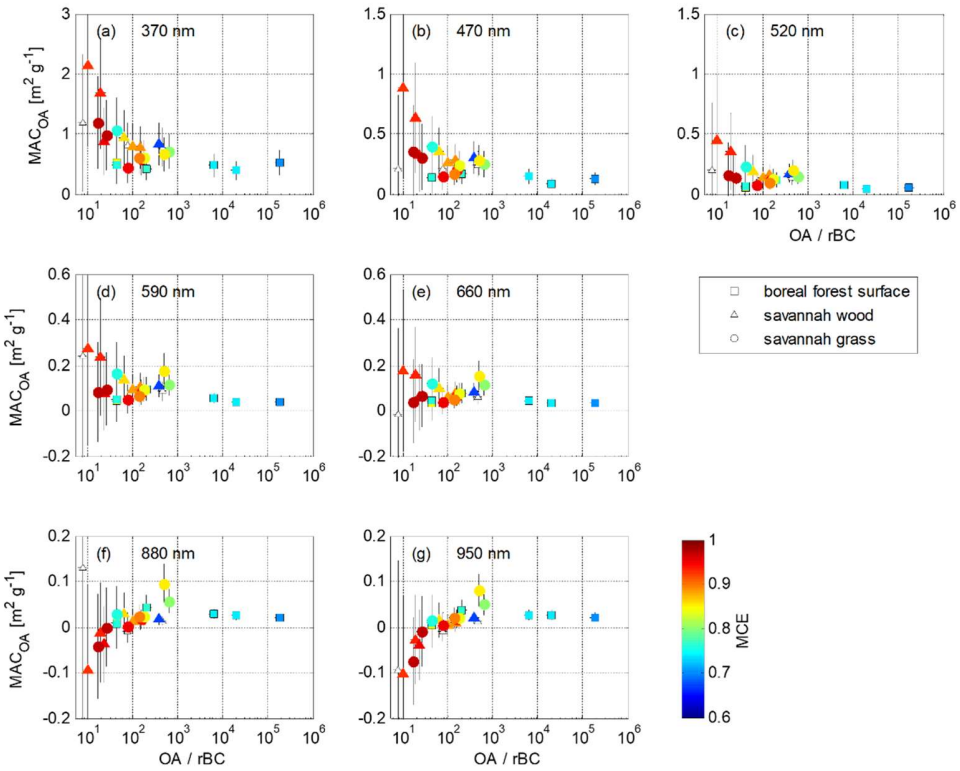

Figure S16. MAC_{OA} as function of OA/rBC ratio at different wavelengths. Error bars indicate measurement uncertainty.

Table S1. Elemental composition of three biomass types. Analysed by Eurofins Environment Testing Finland Oy on 27 June 2022.

Element	Savannah wood	Savannah grass	Boreal forest surface	Measurement uncertainty
C [%]	48.8	43.0	42.8	2 %
H [%]	5.6	5.1	4.5	5 %
N [%]	0.88	0.94	1.47	< 1,2 %: ± 0,1 %-point; > 1,2 %: ± 8 %
S [%]	0.05	0.10	0.13	< 0,1 %: ± 0,01 %-point; > 0,1 %: ± 11 %
Cl [%]	0.075	0.072	0.016	27 %
F [%]	<0.001	<0.001	0.003	45 %
Ca [ppm]	9400	1500	8500	12 %
Mg [ppm]	1100	620	2100	20 %
Na [ppm]	<50	<50	5400	22 %
K [ppm]	5100	3000	4400	14 %
P [ppm]	350	480	1000	14 %

Table S2. List of instrumentation in the BASFAA measurement campaign.

Sampling point	Measured quantity	Instrument	Data presented in this study
Chamber or feeding line after diluters	CO, CO2, CH4, H2O	Picarro G2401	yes
Chamber	VOCs	Vocus-PTR; Tofwerk AG, Aerodyne Research Inc.; Krechmer et al. (2018)	yes
Chamber	O3	Thermo Scientific 49i	no
Chamber	SO2	Thermo Scientific 43i	no
Chamber	NO, NO2	Thermo Scientific 42i	no
Chamber	Size-resolved chemical composition and mass concentration of submicron non-refractory aerosol particles	online high-resolution time-of-flight aerosol mass spectrometer (HR-ToF-AMS) DeCarlo et al. (2006)	yes
Chamber	rBC size distribution	single-particle soot photometer (SP2)	yes
Chamber	aerosol particle volatility distribution, gas and particle chemical composition	Filter Inlet for Gases and AEROsols (FIGAERO, Lopez-Hilfiker et al., 2014; Bannan et al. 2019; Ylisirniö et al., 2021) coupled with a time-of-flight chemical ionization mass spectrometer (ToF-CIMS, Tofwerk AG, Aerodyne Research Inc.)	yes
Chamber	polycyclic aromatic hydrocarbons (PAHs); aerosol particle chemical composition	a novel instrument for single-particle mass spectrometry (SPMS); PhotonLIZA, Photonion GmbH, Germany, Schade et al. (2019)	yes
Chamber	aerosol particle number size distribution	scanning mobility particle sizer (SMPS), TSI model 3082	yes
Chamber	size-resolved aerosol particle effective density	Aerosol Particle Mass analyser (APM), Kanomax model 3602 combined with a SMPS (TSI model 3082)	yes
Chamber	Aerosol particle scattering and backscattering coefficients (b_{scat} and b_{bsca}) at	AirPhoton IN102 integrating nephelometer	yes

	wavelengths of 450 nm, 532 nm and 632 nm		
Chamber	Aerosol particle absorption coefficient (b_{abs}) at wavelengths of 370 nm, 470 nm, 520 nm, 590 nm, 660 nm, 880 nm and 950 nm	aethalometer, Magee Scientific model AE-42	yes
Chamber	size-resolved cloud condensation nuclei (CCN) concentration	CCN counter (CCNc), DMT model CCN-100 coupled with a Vienna-type DMA and a condensation particle counter (TSI model 3775)	no
Chamber	Ice nuclei concentration	a modified SPectrometer for Ice Nuclei (SPIN), Welti et al. (2020)	no
Chamber	OC, EC	off-line filter collection	no
Chamber	VOCs	off-line adsorber tube collection	no
Stack	CO, CO2, VOCs	Fourier transform infrared spectrometer (FTIR), Gasmet Technologies Inc.	no
Stack	CO, CO2	Siemens ULTRAMAT 23	no
Stack	organic aerosol absorption	off-line filter collection for UV-vis spectrophotometer analysis, Mukherjee et al. (2025)	no
Feeding line after diluters	aerosol particle number size distribution	fast mobility particle sizer (FMPS), TSI model 3091	no

Table S3. Fitted bimodal log-normal size distribution parameters for the three different MCE ranges and three biomass types in Fig. 7.

MCE	0.94–0.96			0.83–0.86			< 0.75		
	N [cm^{-3}]	μ [nm]	σ	N [cm^{-3}]	μ [nm]	σ	N [cm^{-3}]	μ [nm]	σ
Savannah	1875	47.1	1.61	328	47.8	1.61	139	50.1	1.84
wood	137	151	1.49	309	107	1.86	238	128	1.66
Savannah	2435	44.8	1.64	627	50.0	1.54			
grass	30.7	272	1.56	196	119	1.86			
Boreal forest				951	36.8	1.83	178	102	2.24
surface				275	80.0	2.29	12.5	147	1.24

References

Bond, T. C., Doherty, S. J., Fahey, D. W., Forster, P. M., Berntsen, T., DeAngelo, B. J., et al. (2013). Bounding the role of black carbon in the climate system: A scientific assessment. *Journal of Geophysical Research: Atmospheres*, *118*(11), 5380–5552. https://doi.org/10.1002/jgrd.50171

Bond, Tami C., & Bergstrom, R. W. (2006). Light Absorption by Carbonaceous Particles: An Investigative Review. *Aerosol Science and Technology*, *40*(1), 27–67. https://doi.org/10.1080/02786820500421521

Gyawali, M., Arnott, W. P., Lewis, K., & Moosmüller, H. (2009). In situ aerosol optics in Reno, NV, USA during and after the summer 2008 California wildfires and the influence of absorbing and non-absorbing organic coatings on spectral light absorption. *Atmospheric Chemistry and Physics*, *9*(20), 8007–8015. https://doi.org/10.5194/acp-9-8007-2009

Luo, J., Li, Z., Qiu, J., Zhang, Y., Fan, C., Li, L., et al. (2023). The Simulated Source Apportionment of Light Absorbing Aerosols: Effects of Microphysical Properties of Partially-Coated Black Carbon. *Journal of Geophysical Research: Atmospheres*, *128*(10), e2022JD037291. https://doi.org/10.1029/2022JD037291

Mukherjee, A., Hartikainen, A., Somero, M., Luostari, V., Ihalainen, M., Rüger, C. P., et al. (2025). Brown carbon emissions from laboratory combustion of Eurasian arctic-boreal and South African savanna biomass. *Atmospheric Chemistry and Physics*, *25*(22), 16747–16774. https://doi.org/10.5194/acp-25-16747-2025

Virkkula, A. (2021). Modeled source apportionment of black carbon particles coated with a light-scattering shell. *Atmospheric Measurement Techniques*, *14*(5), 3707–3719. https://doi.org/10.5194/amt-14-3707-2021

Zotter, P., Herich, H., Gysel, M., El-Haddad, I., Zhang, Y., Močnik, G., et al. (2017). Evaluation of the absorption Ångström exponents for traffic and wood burning in the Aethalometer-based source apportionment using radiocarbon measurements of ambient aerosol. *Atmospheric Chemistry and Physics*, *17*(6), 4229–4249. https://doi.org/10.5194/acp-17-4229-2017